Current distribution and conductance quantization in the integer quantum Hall regime

2003 J. Phys.: Condens. Matter 15 L377

(http://iopscience.iop.org/0953-8984/15/24/104)

INSTITUTE OF PHYSICS PUBLISHING JOURNAL OF PHYSICS: CONDENSED MATTER

J. Phys.: Condens. Matter **15** (2003) L377–L383 PII: S0953-8984(03)63292-3

LETTER TO THE EDITOR

Current distribution and conductance quantization in the integer quantum Hall regime

Alessandro Cresti[1], **Riccardo Farchioni**[1], **Giuseppe Grosso**[1] **and Giuseppe Pastori Parravicini**[2]

[1] NEST-INFM and Dipartimento di Fisica 'E Fermi', Università di Pisa, via F Buonarroti 2, I-56127 Pisa, Italy
[2] NEST-INFM and Dipartimento di Fisica 'A Volta', Università di Pavia, via A Bassi 6, I-27100 Pavia, Italy

E-mail: grosso@df.unipi.it

Received 12 May 2003
Published 6 June 2003
Online at stacks.iop.org/JPhysCM/15/L377

Abstract

Charge transport of a two-dimensional electron gas in the presence of a magnetic field is studied by means of the Keldysh–Green function formalism and the tight-binding method. We evaluate the spatial distributions of persistent (equilibrium) and transport (nonequilibrium) currents, and give a vivid picture of their profiles. In the quantum Hall regime, we find exact conductance quantization both for persistent currents and for transport currents, even in the presence of impurity scattering centres and moderate disorder.

About 20 years ago, the discovery of the integer quantum Hall effect [1] opened a new area of research and has led to extensive investigations on the subject. The most spectacular experimental feature and theoretical challenge is the perfect quantization of the Hall conductance of a two-dimensional electron gas in integer multiples of $2e^2/h$, and its universality regardless of the type of mesoscopic device under investigation, degree of disorder, impurities, etc. The interpretation of transport of two-dimensional conductors in magnetic fields has progressed rapidly [2]. In analogy with currents in a superconductor, Laughlin [3] proposed that conductance quantization was entailed by the long-range phase rigidity of wavefunctions. Halperin [4] pointed out the importance of current-carrying electron states localized at opposite edges of the conducting sample. A major breakthrough in the explanation of the quantum Hall effect has been given by Büttiker [5] in terms of the suppression of elastic or inelastic backscattering, whenever the carriers are moving on opposite edges because of the influence of high magnetic fields. The commonly accepted explanation of the well defined plateaus in the quantum Hall resistance resides in the net spatial separation of edge states supporting right- and left-moving carriers, so the probability of scattering of electrons between states of reverse direction is vanishingly small (see also ch 4 of [6]).

In this letter we investigate the spatial distribution of currents in a two-dimensional electron gas threaded by a magnetic field, and provide a vivid picture of the carriers flowing on the edges of the wire. We find that *both persistent currents and transport currents exhibit exact conductance quantization in the integer quantum Hall regime*; this is true both for ideal samples without disorder and in the presence of impurities, disorder, border irregularities, and other defects.

Model calculations of conductance are often based on the solution of the Schrödinger equation for a particle in a magnetic field with contributions from additional potentials [7]. The other very popular complementary approach is based on the tight-binding formalism [8], which has been a valuable tool mainly for investigating situations where the magnetic flux Φ through a plaquette is comparable with the flux quantum $\Phi_0 = hc/e$. The tight-binding formalism can easily include scattering potentials, but the physics it describes for $\Phi \sim \Phi_0$ entails unrealistically strong magnetic fields applied to the sample. A novelty of the present calculation is adopting the tight-binding framework for the description of a quantum wire in the 'continuum limit', characterized by $\Phi/\Phi_0 \ll 1$, arbitrary longitudinal extension, and sufficiently large transverse width. In this way we achieve a flexible tool, able to describe Landau level formation at realistic magnetic fields, and, at the same time, able to handle quite efficiently impurity scattering processes in the sample. The study of the spatial location of the currents is performed within the nonequilibrium Keldysh Green function formalism [9, 10]; appropriate elaborations [11] exploit the localized nature of the basis functions and provide an extremely accurate investigation tool.

The basis mesoscopic structure under study is a planar lattice of periodicity a, dimensions $L_x = N_x a$ and $L_y = N_y a$, threaded by a uniform perpendicular magnetic field. The number N_x of unit cells in the x-direction is arbitrarily large, while a number N_y of about hundred is found more than sufficient to mimic the continuum limit of the effective-mass approximation. When the first Landau gauge is chosen for the description of the magnetic field, the one-electron Hamiltonian of the lattice model can be written in the form

$$H = \sum_{m,\nu} E_0 |\phi_{m\nu}\rangle\langle\phi_{m\nu}| + t \sum_{m,\nu} [|\phi_{m\nu+1}\rangle\langle\phi_{m\nu}| + |\phi_{m\nu}\rangle\langle\phi_{m\nu+1}|] + t \sum_{m,\nu} [\mathrm{e}^{\mathrm{i}\alpha\nu} |\phi_{m\nu}\rangle\langle\phi_{m+1\nu}| + \mathrm{e}^{-\mathrm{i}\alpha\nu} |\phi_{m+1\nu}\rangle\langle\phi_{m\nu}|], \tag{1}$$

where m is the site index in the x-direction and ν is the chain index in the y-direction, $t < 0$ is the nearest-neighbour hopping parameter, E_0 is the site energy, and the uniform magnetic field B is introduced through the Peierls phase factor $\alpha = 2\pi\Phi(B)/\Phi_0$ with $\Phi(B) = Ba^2$. Additional terms, diagonal in the site representation, are later added to the Hamiltonian (1) to represent the presence of impurities or effect of disorder.

The perfect wire, described by the Hamiltonian (1), is invariant for translations in the x-direction; it is thus convenient, as in tight-binding calculations, to use as basis functions the Bloch sums $\{|\Phi_{\nu k_x}\rangle\}$ built with the localized orbitals belonging to the νth chain of the wire. For any k_x in the first Brillouin zone this leads to the Harper Hamiltonian [12]

$$H(k_x) = \sum_{\nu} 2t \cos(k_x a + \nu\alpha) |\Phi_{\nu k_x}\rangle\langle\Phi_{\nu k_x}| + t \sum_{\nu} [|\Phi_{\nu k_x}\rangle\langle\Phi_{\nu+1 k_x}| + |\Phi_{\nu+1 k_x}\rangle\langle\Phi_{\nu k_x}|]. \tag{2}$$

From the Green function of the Hamiltonian (2), the eigenvalues and density of states can be worked out in a straightforward way. In the presence of impurities or disorder, the Hamiltonian (1), with appropriate additional terms, is handled with standard renormalization procedures [13, 14].

In the following, we consider preliminarily a perfect wire where $\nu = -50, \ldots, 50$ runs over $N_y = 101$ horizontal infinite chains, with site energies $E_0 = 0$, hopping

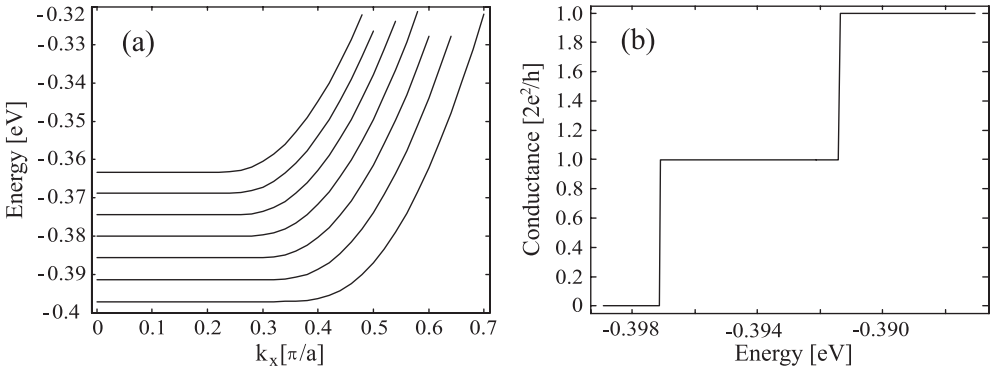

Figure 1. (a) Seven lower-energy magnetic bands of the ideal wire described in the text, as functions of the longitudinal wavevector k_x. (b) Total conductance for Fermi energies in the range $(-0.398, -0.388$ eV). Each jump in the conductance corresponds to the Fermi level intersecting a new magnetic band.

energies $t = -0.1$ eV, bandwidth $8|t|$, effective mass $m^* = 0.1\ m_0$, and lattice parameter $a = \hbar(2m^*|t|)^{-1/2} \simeq 20$ Å. For a magnetic field of 5 T the eigenvalues of the Hamiltonian (2) are reported in figure 1(a). It can be noticed that in the central part of the Brillouin zone the magnetic bands are flat and correspond to bulk Landau levels. The separation between successive Landau levels is $\simeq$5.8 meV in agreement with the estimate in the effective-mass limit. As k_x approaches the border of the Brillouin zone, the energies of the bands rise because the corresponding states approach the physical edge of the wire.

The microscopic currents along each bond of the mesoscopic system are evaluated by means of the Keldysh–Green function framework. The tunnelling current from site $i = (m, \nu)$ to site $j = (m', \nu')$ in steady-state conditions is given by the expression [9, 10]

$$I_{ij} = \frac{2(-e)}{\hbar} \int \frac{\mathrm{d}E}{2\pi} [t_{ij} G^<_{ji} - t_{ji} G^<_{ij}] \tag{3}$$

where $G^<$ is the less-than nonequilibrium Green function of the electronic system, and the factor 2 is included to consider spin degeneracy.

We have shown elsewhere [11] that the general relation (3) leads to the following expression for the site-to-site local currents from the $(m-1)$th column to the mth column:

$$I_{m-1\nu,m\nu} = \frac{2(-e)}{\hbar} \int \frac{\mathrm{d}E}{2\pi} [(-f_L) A^{(m)}_{\nu,\nu} - \mathrm{i}(f_L - f_R) B^{(m)}_{\nu,\nu}]. \tag{4}$$

In equation (4), f_L and f_R are the Fermi–Dirac distribution functions (at $T = 0$ K) of the left and right reservoirs, kept at the chemical potentials μ_L and μ_R. The zero-trace operator

$$A^{(m)} = G^R \Sigma^{R(left)} + \Sigma^{A(left)} G^A - \Sigma^{R(left)} G^R - G^A \Sigma^{A(left)} \tag{5a}$$

defines *persistent currents* (assuming without loss of generality $\mu_L < \mu_R$), while

$$B^{(m)} = G^R \Gamma^{(right)} G^A \Sigma^{A(left)} - \Sigma^{R(left)} G^R \Gamma^{(right)} G^A \tag{5b}$$

defines *transport currents*; all the matrices of equations (5) refer to the N_y sites of the mth column and have rank equal to N_y. Performing the trace over the chain index ν we recover for the *total current* through the device the standard Büttiker–Landauer two-terminal expression

$$I^{(total)} = \frac{2(-e)}{\hbar} \int \mathrm{d}E\, (f_L - f_R)\, \mathrm{Tr}[G^R \Gamma^{(right)} G^A \Gamma^{(left)}], \tag{6}$$

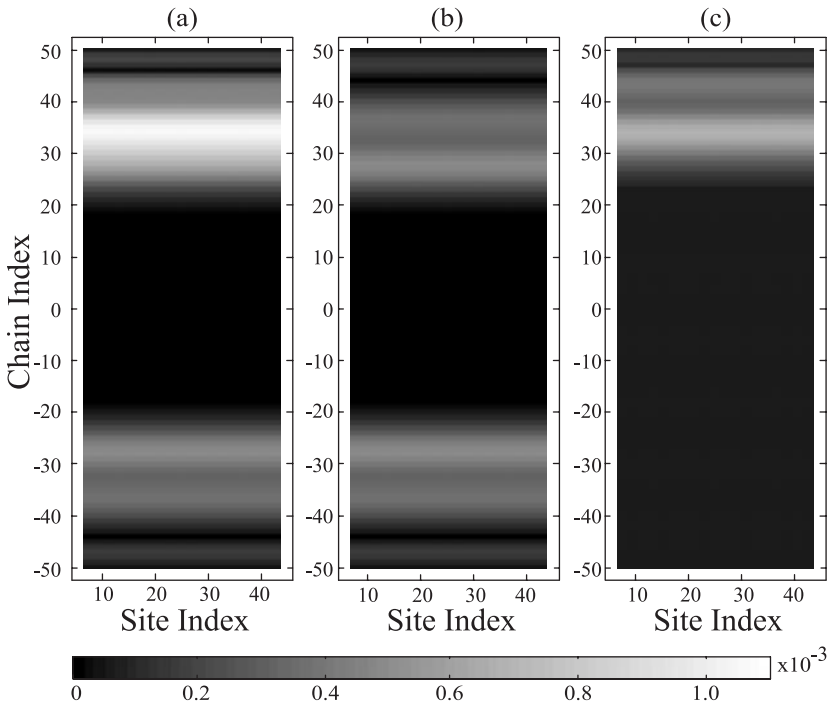

Figure 2. Spatial distribution of currents through a section of the wire of figure 1. The left chemical potential equals −0.391 eV, just above the second Landau level, and the right chemical potential equals −0.387 eV, below the third Landau level. (a) Total currents obtained summing the contributions from persistent currents (b) and transport currents (c). The net current flowing in the wire is $2 \times (2e^2/h) \times \Delta V$ where $\Delta V = 4 \times 10^{-3}$ V. The unit on the greyscale is $(2e^2/h) \times 10^{-3}$, and the absolute values of the currents are reported.

where the trace is to be performed on the sites of any chosen column. The retarded self-energies due to the part of the system at the left and at the right of the mth column are defined as

$$\begin{aligned} \Sigma^{R(left)}_{\nu,\nu'} &= t_{m\nu,m-1\nu} g^R_{m-1\nu,m-1\nu'} t_{m-1\nu',m\nu'} \\ \Sigma^{R(right)}_{\nu,\nu'} &= t_{m\nu,m+1\nu} g^R_{m+1\nu,m+1\nu'} t_{m+1\nu',m\nu'} \end{aligned} \tag{7}$$

(and similarly for advanced quantities); moreover, the linewidth matrices Γ are given by

$$\begin{aligned} \Gamma^{(left)} &= \mathrm{i}\Sigma^{R(left)} - \mathrm{i}\Sigma^{A(left)} \\ \Gamma^{(right)} &= \mathrm{i}\Sigma^{R(right)} - \mathrm{i}\Sigma^{A(right)}. \end{aligned} \tag{8}$$

The retarded and advanced Green functions of the whole system are denoted by G^R and G^A, while g^R and g^A are the retarded and advanced Green functions obtained decoupling the column of index m from the rest of the system. The above Green functions have been obtained by the real-space renormalization procedure which has been proved to be of great feasibility and stability within the tight-binding method [13–15] in a large number of mesoscopic systems. In this way, we can evaluate with high accuracy the local and total (differential) conductances $\partial I/\partial V$, where $(-e)V = \mu_R - \mu_L$ for transport currents and $(-e)V = \mu_L$ for persistent currents.

As a preliminary test, we have verified that the total conductance of the ordered wire is perfectly quantized in units of $2e^2/h$ times the number of open magnetic channels. Thus, for

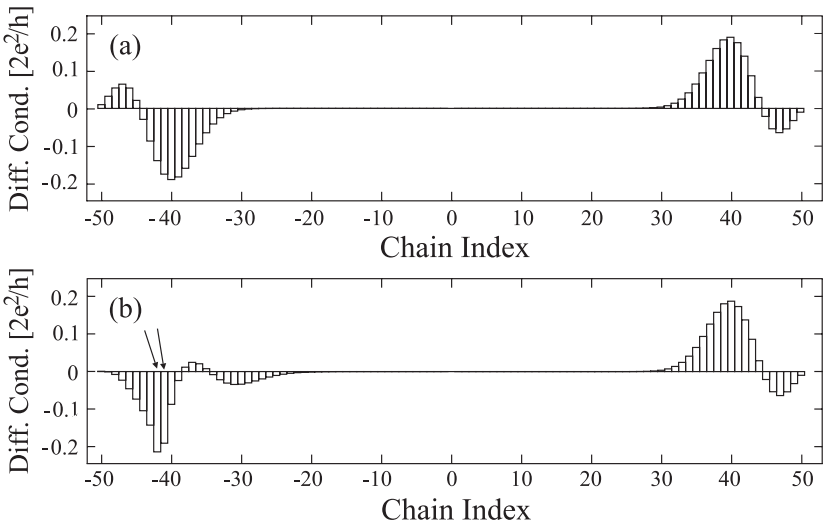

Figure 3. Spatial distribution of the differential conductance of persistent currents in the system of figure 1 at the energy $E = -0.396$ eV. (a) Perfect wire and (b) perfect wire in the presence of two point impurities of strength $\Delta E_0 = t$ in the positions indicated by the arrows.

instance, for $-4|t| < E_F < -0.388$ eV only the lowest two magnetic channels may be active (figure 1(a)), and the corresponding conductance exhibits two steps (figure 1(b)). Moving to higher energies, further steps in the conductance are generated.

It is interesting to look at the regions where currents are distributed: from figure 2(a) it is evident that only edge states support the total current along the wire, which is composed by a persistent (top and down) current (figure 2(b)) and a transport current (figure 2(c)). The states in the bulk of the wire are inactive for charge transport. We examine now in more detail the spatial location of persistent currents, expressed by the zero-trace ('A') contribution of equation (4) where $\mu_L = \mu_R$. As an example, we report in figure 3 the differential conductance of persistent currents at the Fermi energy $E = -0.396$ eV, for the perfect wire and in the presence of impurities. It can be seen that persistent currents flow on opposite sides of the wire. It is important to notice that the two spatially separated contributions obtained summing the conductances over the edge sites are exactly quantized (in units $2e^2/h$); the total conductance exactly gives zero both in the case of figure 3(a) and in the case of figure 3(b). The presence of impurities modifies the shape of the conductance distribution just in the region where the impurities reside, leaving the profile of the opposite edge unperturbed. We note that the conductance remains quantized also in the presence of impurities, until the right- and left-moving carriers remain spatially separated; this can be understood considering that the trace of the persistent currents is always zero, and that the introduced impurities modify only one of the two edge contributions.

To further test the robustness of the conductance quantization versus scattering potentials, we have inserted in the wire an extended disordered region, as specified in figure 4. The conductance profiles exhibit deep modifications and also the formation of vortexes (clearly visible on expanded-scale figures not shown here); but, as long as the flow of persistent currents occurs on spatially separated regions, each contribution to the conductance is exactly quantized in units of $2e^2/h$. The persistent and transport contributions to the conductance tend to equalize in magnitude as the quantum Hall regime is approached.

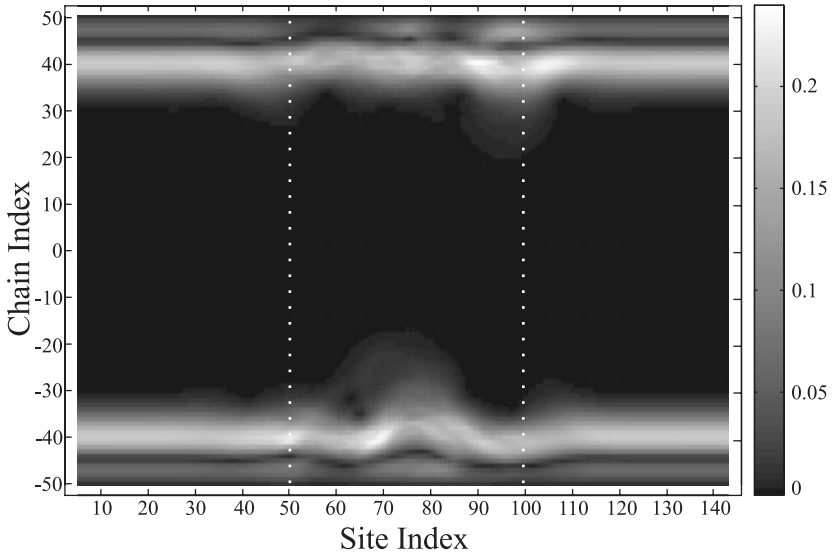

Figure 4. Spatial distribution of the differential conductance (absolute values), at the energy $E = -0.396$ eV, due to the persistent currents in the wire of figure 1. Random distribution of point impurities, with energies $|W| \leqslant 0.2|t|$, is inserted in the region indicated by two dotted vertical lines. The unit of the greyscale is $2e^2/h$.

In conclusion, we have shown the robustness of the exact conductance quantization both for transport currents and for spatially separated persistent currents. The occurrence of the former quantization entails negligible longitudinal potential drop when current flows across the sample; the occurrence of the latter entails exact conductance quantization when the Hall potential develops on the opposite sides of the sample. The picture that we have outlined for the current profiles gives insight into the microscopic mechanisms leading to the exact conductance quantization in the integer quantum Hall regime.

This work was supported in part by MURST-PRIN 2001, by INFM project PAIS-NANOCURR 2003, and by National Enterprise for Nanoscience and Nanotechnology (NEST-INFM).

References

[1] von Klitzing K, Dorda G and Pepper M 1980 *Phys. Rev. Lett.* **45** 494
von Klitzing K 1986 *Rev. Mod. Phys.* **68** 519
[2] Das Sarma S and Pinczuk A (ed) 1997 *Perspectives in Quantum Hall Effects* (New York: Wiley) and references quoted therein
[3] Laughlin R B 1981 *Phys. Rev.* B **23** 5632
[4] Halperin B I 1982 *Phys. Rev.* B **25** 2185
[5] Büttiker M 1988 *Phys. Rev.* B **38** 9375
[6] Datta S 1995 *Electronic Transport in Mesoscopic Systems* (Cambridge: Cambridge University Press)
[7] See for instance
MacDonald A H 1984 *Phys. Rev.* B **29** 6563
Avishai Y, Hatsugai Y and Kohmoto M 1993 *Phys. Rev.* B **47** 9501
Zheng Y and Ando T 2002 *Phys. Rev.* B **66** 085328 and references quoted therein
[8] See for instance
Rammal R, Toulouse G, Jaekel M T and Halperin B I 1983 *Phys. Rev.* B **27** 5142
Schweitzer L, Kramer B and MacKinnon A 1984 *J. Phys. C: Solid State Phys.* **17** 4111

Nonoyama S and Kirczenow G 2002 *Phys. Rev.* B **66** 155334 and references quoted therein
[9] Keldysh L V 1964 *Zh. Eksp. Teor. Fiz.* **47** 1515 (Engl. transl. 1965 *Sov. Phys.–JETP* **20** 1018)
[10] Caroli C, Combescot R, Nozières P and Saint-James D 1971 *J. Phys. C: Solid State Phys.* **4** 916
Caroli C, Combescot R, Nozières P and Saint-James D 1972 *J. Phys. C: Solid State Phys.* **5** 21
[11] Cresti A, Farchioni R, Grosso G and Pastori Parravicini G 2003 *J. Appl. Phys.* at press
[12] Harper P G 1955 *Proc. Phys. Soc.* A **68** 874
[13] Grosso G and Pastori Parravicini G 2000 *Solid State Physics* (London: Academic) and references quoted therein
[14] Farchioni R, Grosso G and Vignolo P 2001 *Recursive Algorithms for Polymeric Chains (Springer Series in Materials Science vol 41)* (Berlin: Springer) 89–125 and references quoted therein
[15] Todorov T N 2002 *J. Phys.: Condens. Matter* **14** 3049